Deoxyribose Conformation in [d(GTATATAC)]$_2$: Evaluation of Sugar Pucker by Simulation of Double-Quantum-Filtered COSY Cross-Peaks†

Uli Schmitz,‡ Gerald Zon,§ and Thomas L. James*,‡

Departments of Pharmaceutical Chemistry and Radiology, University of California, San Francisco, California 94143-0446, and Applied Biosystems, Inc., Foster City, California 94404

Received August 14, 1989; Revised Manuscript Received November 1, 1989

ABSTRACT: Exchangeable and nonexchangeable proton and phosphorus resonances (11.75 T) of [d(GTATATAC)]$_2$ in aqueous solution were assigned by using proton two-dimensional nuclear Overhauser effect (2D NOE) spectra, homonuclear proton double-quantum-filtered COSY (2QF-COSY) spectra, proton spin–lattice relaxation time measurements, and ^{31}P^{1}H heteronuclear shift correlation spectra. Due to the large line widths, it was not possible to directly extract vicinal proton coupling constant values from any spectrum including ECOSY or 2QF-COSY. However, comparison of quantitative 2QF-COSY spectral simulations with experimental spectra enabled elucidation of coupling constants. The scope and limitations of this approach were explored by computation and by use of experimental data. It was found that proton line widths exhibit some variability from one residue to the next as well as from one proton to the next within a residue and the exact line width is critical to accurate evaluation of coupling constants. Experimental 2QF-COSY spectra were not consistent with a rigid deoxyribose conformation for any of the nucleotide residues. A classical two-state model, with rapid jumps between C2′-endo (pseudorotation angle P = 162°) and C3′-endo (P = 9°) conformations, was able to account for the spectral characteristics of terminal residue sugars: 60% C2′-endo and 40% C3′-endo. However, the 2QF-COSY cross-peaks from the -TATATA- core could be simulated only if the classical two-state model was altered such that the dominant conformer had a pseudorotation angle at 144° instead of 162°. In this case, the major conformer amounted to 80–85%. Alternatively, the spectral data were consistent with a three-state model in which C2′-endo and C3′-endo conformations had the largest and smallest populations, respectively, but a third conformer corresponding to C1′-exo (P = 126°) was present, consistent with recent molecular dynamics calculations. This alternative yielded populations of 50% (P = 162°), 35% (P = 126°), and 15% (P = 9°) for the -TATATA- sugars. The spectral results indicate little variation of sugar pucker between T and A. Small differences in cross-peak component intensities and characteristic spectral distortions, however, do suggest some unquantified variation. ^{31}P^{1}H heteronuclear chemical shift correlation spectra manifested alternating chemical shifts and coupling constants suggestive of phosphodiester backbone conformational differences between TA and AT junctions.

Solution structures of oligonucleotides containing tracts with alternating AT sequences are becoming increasingly interesting, since several promoter regions in genes seem to include pertinent TA-rich sequences. X-ray diffraction analyses of polymorphic poly[d(A-T)]·poly[d(A-T)] fibers have lead to several proposed structures, including the wrinkled D-DNA structure, a member of the B-DNA family (Arnott et al., 1983).

This stimulated a study on the solution structure of [d(ATATATATAT)]$_2$ by our group (Suzuki et al., 1986), based on a complete relaxation matrix analysis of proton two-dimensional nuclear Overhauser effect (2D NOE)[1] cross-peak intensities and molecular mechanics calculations to disclose a structure almost identical with wrinkled D-DNA. Similar studies were carried out on [d(GGTATACC)]$_2$, revealing a B-DNA-like structure for the GG/CC part and a wrinkled D-DNA-type structure for the TATA/ATAT moiety (Jamin et al., 1985; Zhou et al., 1987). X-ray crystallography, in contrast, revealed an A-DNA structure for this octamer (Shakked et al., 1981, 1983).

Compared to regular B-DNA, wrinkled D-DNA is a lean, overwound helix with a small van der Waals diameter of 21 Å, generating a shallow major groove and a deep narrow minor groove. There is marked propeller twisting in the base pairs. Alternating torsion angles at AT and TA junctions reflect the wrinkled character. As the backbone torsion angles are related to deoxyribose sugar pucker, some alternation in sugar pucker is also expected. However, NOE-based structures predominantly reflect base pair geometry; accurate representation of sugar pucker is not guaranteed. Coupling constant analysis of deoxyribose protons leading to knowledge of dihedral angles, and thus to sugar conformational assignment, should be most appropriate. However, [d(ATATATATAT)]$_2$ was not amenable to this approach as the proton resonance lines are too broad to reliably determine coupling constants.

Auspicious line widths enabled a vicinal coupling constant and sugar puckering analysis of [d(GGTATACC)]$_2$ (Zhou et al., 1988). The GG/CC moiety was found to be different

† Supported by National Institutes of Health Grants GM 39247 and RR 01695 and by a NATO fellowship donated by the Deutscher Akademischer Austauschdienst to U.S.

* Address correspondence to this author at the Department of Pharmaceutical Chemistry, University of California, San Francisco.

‡ University of California, San Francisco.

§ Applied Biosystems, Inc.

[1] Abbreviations: NOE, nuclear Overhauser effect; 2D NOE, two-dimensional NOE; FID, free induction decay; 1D, one dimensional; 2D, two dimensional; COSY, correlated spectroscopy; 2QF-COSY, double-quantum-filtered COSY; ppm, parts per million; P_N, pseudorotation phase angle of a conformer representing the N range; P_S, pseudorotation phase angle of a conformer representing the S range; ECOSY, exclusive COSY; PECOSY, primitive exclusive COSY; EGTA, [ethylenebis(oxyethylenenitrilo)]tetraacetic acid; HSC, heteronuclear shift correlation; T_1, spin–lattice relaxation time; TMP, thymidine monophosphate;

0006-2960/90/0429-2357$02.50/0

from the TATA/ATAT core of the oligonucleotide, having a somewhat greater conformational flexibility. However, a distinct sequence dependence of sugar pucker could not be detected. These findings lead to the present investigation of $[d(GTATATAC)]_2$, which exhibits an alternating purine-pyrimidine sequence very similar to $[d(ATATATATAT)]_2$. Compared to the latter, however, $[d(GTATATAC)]_2$ was expected to have narrower lines because (a) it is shorter and (b) possible concatenation of more than two oligonucleotides is prohibited by the terminal GC base pair, thus enabling a coupling constant analysis.

Crystal structures show that the vast majority of the B-DNA-like oligonucleotides display a sugar pucker within a narrow range close to the C2′-endo conformation described by a pseudorotation phase angle of $P = 137–94°$ (de Leeuw et al., 1980). X-ray diffraction data and NOE-based studies present sugar pucker generally in a static way. However, NOE data do not necessarily have to be interpreted in terms of one rigid conformer. In fact, the energy differences between separate conformers in the pseudorotation pathway are quite small. Several NMR coupling constant studies have shown that equilibria involving two rapidly interconverting conformers describe sugar pucker quite adequately (de Leeuw & Altona, 1982, 1983).

A fairly accurate determination of vicinal coupling constants involving H1′, H2′, H2″, H3′, and H4′ or sums of coupling constants is necessary to derive pseudorotational parameters and populations of the participating conformers utilizing the two-state model. Most of the methods used to extract coupling constants from NMR spectra are limited by spectral parameters, such as natural line widths and digital resolution. A quantitative simulation method has been developed recently (Widmer & Wüthrich, 1986; Celda et al., 1989) which may enable determination of coupling constants even when the line width exceeds the value of the coupling constants.

This paper explores the value as well as the limitations of using quantitative spectral simulations, specifically of 2QF-COSY spectra, to extract vicinal coupling constants when line widths are significant. In particular, the method is applied to $[d(GTATATAC)]_2$ following the nearly complete assignment of exchangeable and nonexchangeable proton resonances.

Materials and Methods

The octanucleotide $[d(GTATATAC)]_2$ was synthesized by a solid-state phosphoramidite method and purified as described previously (Broido et al., 1984). Its purity was checked by HPLC, by base composition analysis, and by ^1H and ^{31}P NMR. The sample was dissolved in a boric acid buffer solution (50 mM borate, 100 mM NaCl, and 0.2 mM EGTA, pH 8) to give a final concentration of 1.7 mM in duplex, lyophilized 3 times from ^2H_2O, and finally dissolved in 0.4 mL of 99.996% ^2H_2O for experiments with nonexchangeable protons (2D NOE, 2QF-COSY, ECOSY). The solvent was 90% H_2O/10% ^2H_2O to obtain spectra with exchangeable proton resonances. A different sample, 1.9 mM in duplex dissolved in a cacodylate buffer (10 mM cacodylate, 100 mM NaCl, and 0.5 mM EGTA, pH 7), was used to obtain the 2D $^{31}P^1H$ heteronuclear shift correlation spectra.

All ^1H NMR measurements were carried out at 15 °C on a 500-MHz spectrometer (General Electric GN-500) and processed with locally written software. 2QF-COSY spectra were obtained with a time proportional phase incrementation scheme (Marion & Wüthrich, 1983). The carrier frequency was set at the HDO peak frequency. Sweep width in both dimensions was 4000 Hz. FID's (4K data points) were acquired with 64 scans at each of 800 t_1 values, representing acquisition times of 100 and 512 ms in t_1 and t_2, respectively. Apodization with shifted sine bells and zero-filling in both dimensions was used to obtain a final data set of 4K × 1K with a digital resolution of 0.9 Hz/point in ω_2 and 3.9 Hz/point in ω_1. The ECOSY experiment was carried out according to a recently described pulse sequence (Griesinger et al., 1987), and data processing was practically identical with the 2QF-COSY experiment. Pure absorption 2D NOE spectra were acquired by using a pulse sequence (Kumar et al., 1980) with alternate block accumulation and phase-cycling (States et al., 1982). The 2D NOE experiment in 90% H_2O/10% ^2H_2O solution was carried out with a $1\bar{3}3\bar{1}$ excitation pulse (Hore et al., 1983), followed by a short homospoil pulse to suppress the water signal. Proton excitation was centered at 10.5 ppm, halfway between imino proton and amino–aromatic proton regions. For both cases, the mixing time was 200 ms, and the repetition time was 10 s. FID's (4K data points) were acquired with 16 scans at each of 400 t_1 values. Apodization with double Gaussian–Lorentzian multiplication and zero-filling in both dimensions was used to obtain 4K × 1K datasets. Digital resolution was 0.9 Hz/point in ω_2 and 3.9 Hz/point in ω_1 for 2D NOE spectra from the ^2H_2O sample and 3.4 Hz/point in ω_2 and 13.6 Hz/point in ω_1 for the 2D NOE spectra from 90% H_2O/10% ^2H_2O solution.

The proton-detected $^{31}P^1H$ heteronuclear shift correlation experiment was carried out according to a well-described technique (Maudsley & Ernst, 1977; Williamson & Bax, 1980) with modified phase cycling. FID's (4K data points) were acquired for 64 t_1 values. Apodization with double Gaussian–Lorentzian multiplication and zero-filling in both dimensions was used to obtain a final data set of 4K × 512 with a digital resolution of 0.9 Hz/point in ω_2 and 1.0 Hz/point in ω_1.

The inversion–recovery method utilizing a 180° composite pulse was used for T_1 relaxation time estimation (Freeman et al., 1980).

SPHINX and LINSHA programs (Widmer & Wüthrich, 1986) were used to simulate 2QF-COSY cross-peaks for the deoxyribose spin system involving H1′, H2′, H2″, H3′, H4′ and the phosphorus ^{31}P spin, coupled to H3′.

SPHINX calculated stick spectra, treating all proton spins as strongly coupled nuclei. Line shape was added to the stick spectra using LINSHA. Digital resolution, apodization functions, truncations of the FID, and natural line widths were incorporated into the LINSHA calculations. Proton coupling constants for specific deoxyribose conformers were taken from the literature (Rinkel & Altona, 1982).

Results and Discussion

Assignment of Exchangeable and Nonexchangeable Resonances. Nonexchangeable protons were assigned in a sequential manner using 2D NOE and 2QF-COSY spectra following the strategy described in earlier work [e.g., see Feigon et al. (1982, 1983), Scheek et al. (1983, 1984), and Broido et al. (1984)]. Chemical shifts are listed in Table I.

T_1 relaxation time estimations, given in Table II, also aided in assigning resonances. Besides identification of the adenine H2 resonances due to their rather long T_1 values, even their assignment to specific residues could be made. Adenine H2 protons, though not exhibiting any reliable NOE interactions with sugar protons, showed several interstrand cross-peaks among one another. This indicates that the middle one of the three adenine H2 resonances, manifesting cross-peaks to the other two, must belong to A3 H2, since the structure of the right-handed double helix (Figure 1) exclusively allows the NOE interactions A7 H2–A3 H2 and A3 H2–A5 H2. For

Table I: Chemical Shifts of (ppm) [d(GTATATAC)]$_2$[a]

position	G1	T2	A3	T4	A5	T6	A7	C8
H1′	5.98	5.91	6.34	5.73	6.25	5.71	6.25	6.06
H2′	2.68	2.32	2.72	2.15	2.63	2.04	2.63	2.14
H2″	2.79	2.64	3.01	2.53	2.92	2.44	2.87	2.16
H3′	4.83	4.97	5.08	4.93	5.03	4.90	5.04	4.49
H4′	4.24	4.31	4.48	4.25	4.44	4.21	4.43	4.03
H5′	3.82	4.16	4.26	4.33	4.20–4.22	4.31	4.20/4.22	4.08
H5″	3.77	4.10–4.17	4.18	4.20	4.20–4.22	4.16	4.20/4.22	4.27
H2			7.34		7.17		7.45	
H5								5.18
H6		7.45		7.23		7.21		7.31
H8	7.91		8.37		8.26		8.23	
CH_3		1.38		1.47		1.42		
NH	12.7 br	13.54		13.21		13.39		
NH_2[b]			7.65		7.55			8.04
NH_2[c]								6.66

[a] Unassigned amino resonances: 6.84 ppm, 7.01 ppm. [b] Amino proton involved in hydrogen bond. [c] Amino proton not involved in hydrogen bond.

Table II: Spin–Lattice (T_1) Relaxation Times of Some Protons in [d(GTATATAC)]$_2$ at 15 °C

proton	T_1 (s)	proton	T_1 (s)
T2 CH_3	1.6	G1 H1′	1.6
T4 CH_3	2.0	all other H1′	1.9
T6 CH_3	2.0	all H2′ and H2″	1.3–1.4
G1 H8	1.6	all H3′, H4′, H5′, and H5″	1.3–1.7
A3 H8	2.0	G1 H5′/H5″	1.0
A5 H8	2.0		
A7 H8	1.9		
A3 H2	3.5		
A5 H2	3.5		
A7 H2	3.6		
other aromatic H	1.7–2.0		

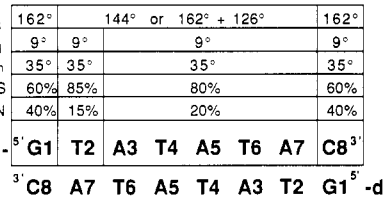

FIGURE 1: Structure of the self-complementary GTATATAC duplex and description of the sugar puckers found from the present studies. P_S and P_N are the pseudorotation phase angles of the conformers representing the S range and N range of the pseudorotation cycle. Φ_m is the amplitude of pucker. % S and % N give the percentage of the S and N conformers in a dynamic model. For the core of the duplex, two dynamic models could fit the data: a two-state model with rapid jumps between an N conformer (P_N = 9°) and S conformer (P_S = 144°) or a three-state model with rapid jumps among an N conformer and two S conformers one with P_S = 162° and the other with P_S = 126°.

a particular proton type (e.g., A H2), deviations in T_1 relaxation times may indicate either different mobilities in different parts of the molecule, different dipole–dipole interactions, or both. The downfield adenine H2 resonance exhibits a slightly shorter T_1 relaxation time than the other two, suggesting it belongs to A7 H2, which is located adjacent to the terminal GC base pair and may reflect some degree of fraying of that terminal pair. Among the T2, T4, and T6 methyl group resonances, the T4 and T6 methyls are in an all-adenine environment, but the T2 methyl is adjacent to the terminal GC base pair, suggesting the resonances with the same T_1 value are from T4 and T6. The T2 methyl group apparently exhibits a significantly shorter T_1 value. The shortest T_1 relaxation time (1.0 s) was found for G1 H5′/H5″, which is likely to belong to the most flexible part of the molecule.

Assignment of the exchangeable protons was made as described previously (Boelens et al., 1985; Zhou et al., 1988). The 2D NOE spectrum (τ_m = 200 ms) obtained in 90% H_2O/10% ^2H_2O exhibits four large downfield cross-peaks with the water signal (Figure 2), corresponding to the four imino protons of G1, T2, T4, and T6 observed in the 1D NMR spectra. However, only the two sharper inner resonances show additional cross-peaks: (a) to amino protons (7.65 and 7.55 ppm) involved in Watson–Crick hydrogen bonding; (b) to other sequential imino protons; (c) to adenine H2 protons; and, unexpectedly, (d) to adenine H1′ protons. This latter finding must be confirmed by further NOE studies. Of two imino proton resonances, the one to lower field exhibits three NOE interactions of very different intensity to all three adenine H2 protons. A strong NOE interaction is expected within a base pair, a medium one should arise from the preceding 5′ adenine H2, and a weak peak should originate from the following 3′ adenine H2, reflecting typical distance relations of B-DNA (Wüthrich, 1986). This observed intensity pattern made T4 NH and T6 NH assignments independent from knowing the proper adenine H2 chemical shifts. The commonly employed strategy of assigning the imino proton resonances with help from the adenine H2 resonances was reversed in the present study, since A7 H2 and A5 H2 were only tentatively assigned from the previously mentioned T_1 argument, and stronger proof was given by dipolar coupling to the imino protons. The broader of the two imino proton resonances not exhibiting cross-peaks other than those with the H_2O signal was assigned to G1, consistent with studies on some other GC-terminal oligonucleotides (Zhou et al., 1988; Boelens et al., 1985). Cross-peaks to C8 H5 and to another broad amino proton resonance (6.66 ppm) located the C8 amino proton (8.04 ppm) involved in the GC hydrogen bond. Besides previously described and discussed NOE interactions between adenine H2 protons and H_2O protons (Zhou et al., 1988), water protons exhibit two broad unassigned cross-peaks, hinting at other amino proton resonances, at 6.84 and 7.01 ppm.

Determination of Deoxyribose Pucker in Oligonucleotides by Coupling Constant Analysis. Several methods to determine sugar pucker in oligonucleotides have been described and frequently applied. The well-established relationship between H,H dihedral angles and ^{1}H,^{1}H vicinal coupling constants, known as the modified Karplus equation (Altona, 1982), provides a fairly accurate and straightforward determination of sugar pucker. However, extraction of coupling constant values can become complicated with oligonucleotides due to peak overlap and increased line widths. In addition, even with reasonably accurate and complete sets of vicinal coupling constants, difficulties in interpretation may be encountered whenever there is rapid interconversion between two or more conformers.

Evaluation of 1D NMR spectra or analysis of *J*-resolved

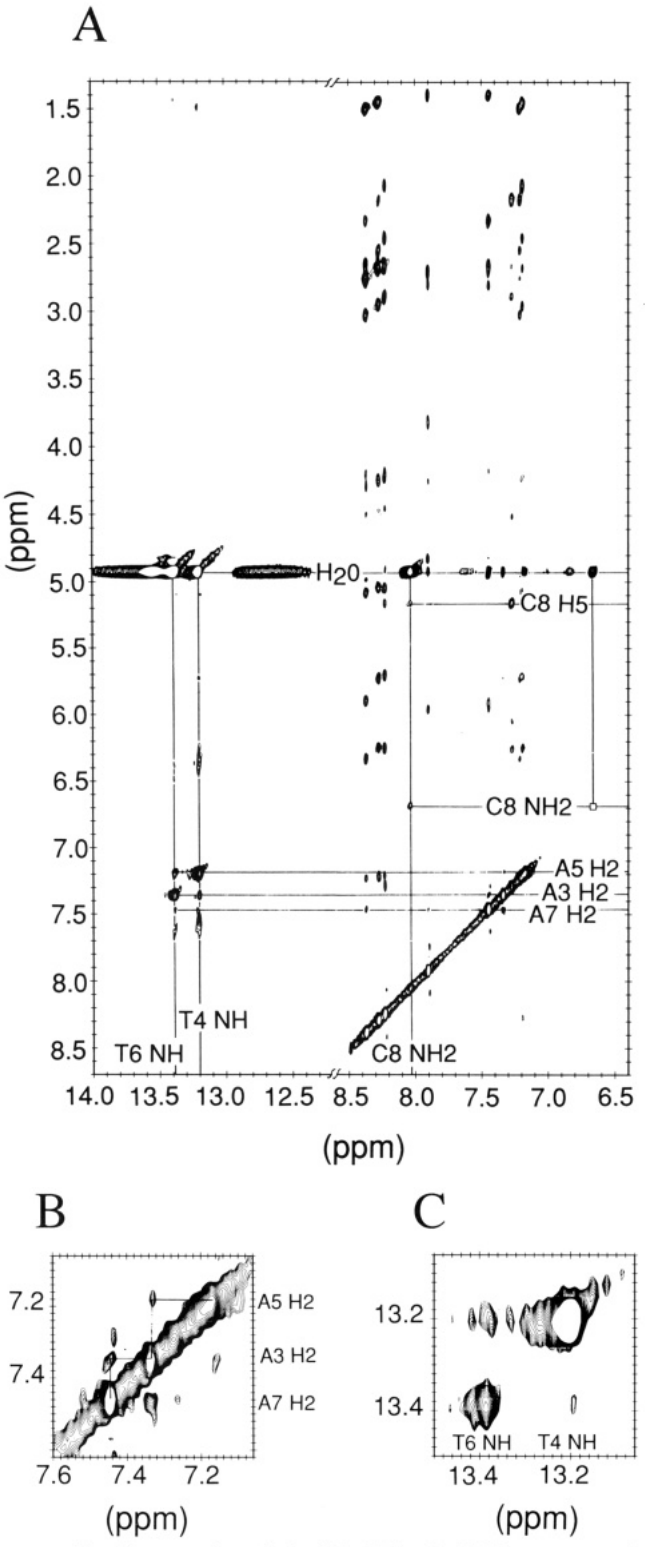

FIGURE 2: Contour plot of the 500-MHz 2D NOE spectrum of $[d(GTATATAC)]_2$ in 90% H_2O/10% ^2H_2O, 15 °C. (A) Portions of the 2D NOE spectrum downfield of the water signal are shown. Some resonances of the exchangeable protons and the adenine H2 protons are labeled. (B) Expanded view of the adenine H2 proton cross-peaks with each other. (C) Expanded view of the imino proton cross-peaks with each other.

2D NMR spectra, even with the DISCO procedure (Kessler et al., 1985), to determine coupling constants, must fail in those cases where large line widths or severe peak overlap distorts peak shapes seriously. Also, the success of 2D NMR editing techniques, e.g., 2QF-COSY (Piantini et al., 1982), ECOSY (Griesinger et al., 1985), and PECOSY (Bax & Lerner, 1988),

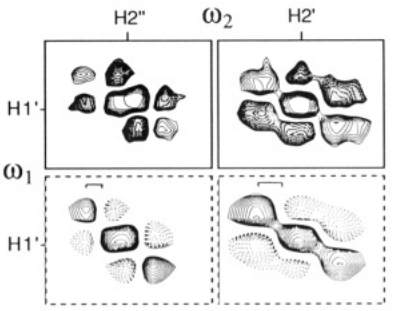

FIGURE 3: Experimental H1′H2″-ω_2 and H1′H2′-ω_2 ECOSY cross-peaks of A3 (solid boxes) and simulation for a line width of 11 Hz in ω_2 and 9 Hz in ω_1 (dashed boxes), using $^3J_{1'2'} = 9.0$ Hz, $^3J_{1'2''} = 6.0$ Hz, and $^2J_{2'2''} = -14.0$ Hz. Negative peaks are indicated by shaded regions or dashed lines, respectively. Distance bars in the simulated peak boxes display the size of the actual active coupling constant used for the simulation.

usually very helpful for coupling constant extraction and their assignment due to their simplified peak patterns, is limited whenever the line width surpasses the magnitude of the splitting. It is well-known that in these cases the observed splittings within a fine structure turn out to be larger than the true coupling constants (Neuhaus et al., 1985). We performed an ECOSY experiment on $[d(GTATATAC)]_2$ and found the results rather unsatisfactory since the observed separations within the fine structures were unreasonably large, and some cross-peaks had distorted shapes. Figure 3 compares an exemplary ECOSY cross-peak (H1′H2′-ω_2) with some quantitative simulations utilizing coupling constants determined by simulations of 2QF-COSY spectra (vide infra). Plots for different line widths clearly show that the aforementioned effects are manifestations of the line-width problem. Once the natural line width is well-established, simulation could yield results matching the experimental ECOSY spectrum.

Another limitation of 2D NMR techniques is the digital resolution, which is generally reported to be ≥0.9 Hz/point after zero-filling in the better resolved dimension. For example, in principle, $^3J_{1'2'}$, $^3J_{1'2''}$, and $^2J_{2'2''}$ should be available from a well-resolved ECOSY spectrum, but the error might extend to twice the digital resolution. However, very accurate values of $^3J_{1'2'}$ and $^3J_{1'2''}$ are required to establish a definite sugar conformation. $^3J_{1'2''}$ in particular is not very sensitive to conformational changes; an error range of ≈1 Hz would accommodate a large variety of different sugar puckers.

A low-resolution COSY technique has been described recently (Hosur et al., 1988; Chary et al., 1988, 1989) which assesses cross-peak intensities to evaluate the relative size of coupling constants, assuming that active coupling is the prevailing factor determining intensities. From our experience, we find that the success of this method is highly dependent on the actual line widths of the pertinent peaks. In the present study, we have found line width, not surprisingly, to vary even within one residue, so some kind of calibration seems to be advisable (vide infra).

If most of the deoxyribose vicinal coupling constants are available, the PSEUROT program (de Leeuw & Altona, 1983) provides a valuable way to calculate the following pucker parameters, assuming a two-conformer equilibrium: pseudorotation phase angle (P) and maximum amplitude of pucker (Φ_m) of the dominant conformer and the ratio of conformers. The pucker parameters of the minor conformer are chosen, not calculated. A recently described graphical method (Rinkel & Altona, 1987) employs sums of coupling constants, often available from partially resolved multiplets in COSY spectra, and coupling constants derivable from H1′ peaks in 1D NMR

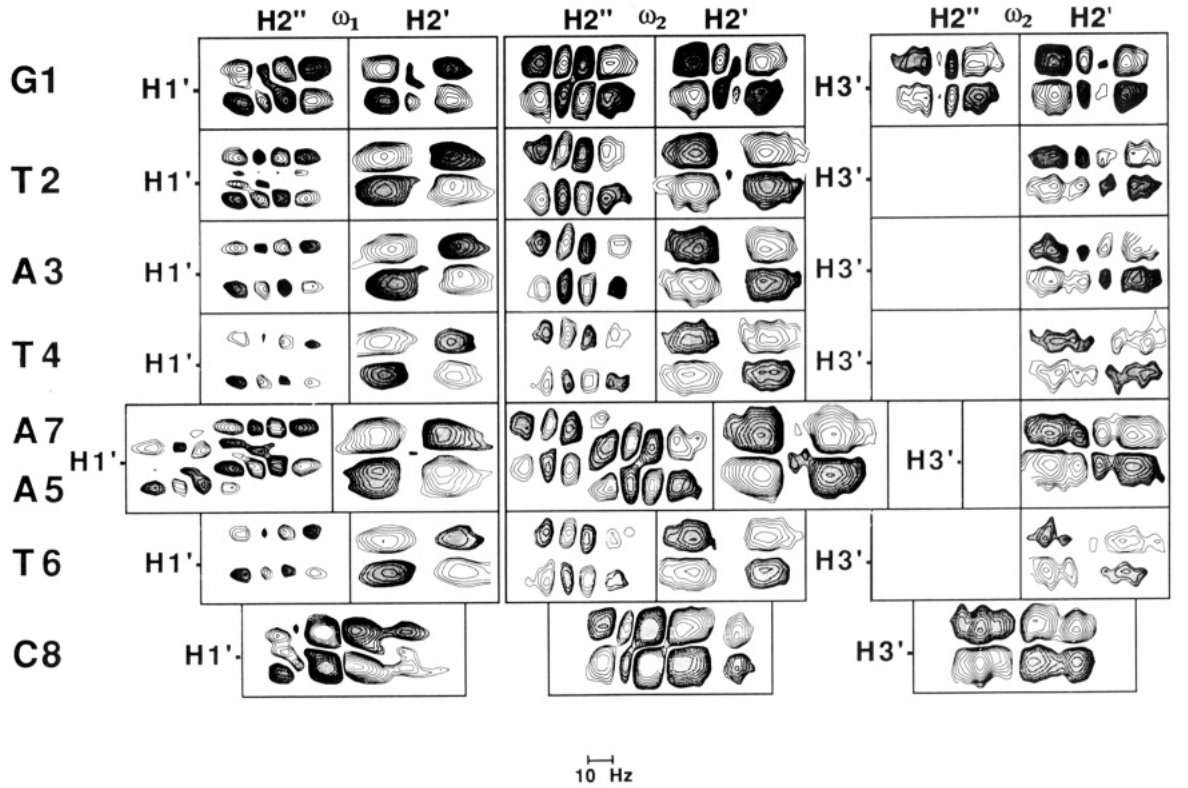

FIGURE 4: Experimental 2QF-COSY cross-peaks of $[d(GTATATAC)]_2$: H1′H2″-ω_1, H1′H2′-ω_1, H1′H2″-ω_2, H1′H2′-ω_2, H3′H2″-ω_2, and H3′H2′-ω_2 from left to right. Digital resolution is 0.9 Hz/point in ω_2 and 3.9 Hz/point in ω_1. Negative peaks are indicated by the shaded regions. Chemical shift positions are indicated by the proton labels H1′, H2′, H2″, and H3′.

spectra, to determine the sugar pucker on the basis of a two-conformer equilibrium.

None of the methods described above could provide the sugar pucker information for $[d(GTATATAC)]_2$, so we tried quantitative simulation of 2QF-COSY cross-peaks, which should be able to account for the considerable line widths encountered as well as digital resolution.

Determination of Deoxyribose Pucker by Quantitative Simulation of 2QF-COSY Cross-Peaks. All experimental 2QF-COSY cross-peaks, which were investigated by spectral simulation, are shown in Figure 4: H1′H2′ and H1′H2″ for ω_1 and ω_2 dimensions and H3′H2′ and H3′H2″ just for the ω_2 dimension. Only cross-peaks of C8 were so strongly overlapped that simulation did not seem promising. A7 H2′ and A5 H2′ are virtually isochronous, but because the shape of the overlapped cross-peaks was so similar to comparable ones (e.g., A3), they were included in the evaluation.

A visual inspection of Figure 4 reveals the pronounced similarity of all related cross-peaks of residues T2 through A7. The terminal nucleotides, G1 and C8, deviate, however. For example, only these two exhibit a H3′H2″ cross-peak. In the case of C8, this is indicated only by intensity assessment. Only the T2 H1′H2″-ω_1 peak displays all 16 expected components of the fine structure belonging to a spin which is coupled to 2 other connected spins. In all other cases, amalgamation and cancellation effects of antiphase peaks are responsible for the reduction to eight, six, or four components only, so that peak-to-peak separations do not represent any of the involved coupling constants.

The least variability is shown by the H1′H2″-ω_2 peaks, all manifesting a similar eight-component pattern. However, the same series of cross-peaks displays a distinct difference between G1, T2, and the central core of the oligonucleotide in the ω_1 dimension, due to different digital resolution for the two spectral dimensions. This demonstrates the necessity of simulating both complements of the 2D NMR spectrum.

Initially, a series of simulations was generated utilizing different rigid sugar puckers, defined by the pseudorotation phase angle P and the pucker amplitude Φ_m (Altona & Sundaralingam, 1972). Coupling constants for $\Phi_m = 35°$ and selected values of P were taken from the literature (Rinkel & Altona, 1987). The corresponding 2QF-COSY cross-peaks were calculated for four different line widths (7, 9, 11, and 13 Hz width at half-height). Figure 5 shows the 9-Hz series of cross-peaks for a range of P values; the range from 90° to 225° is characterized by the absence of the H3′H2″ cross-peak due to an active coupling constant ≤3.5 Hz. Another set of simulations was carried out for several mixtures assuming an equilibrium of two conformers, one with $P_N = 9°$ and $\Phi_m = 35°$ and the other one with $P_S = 162°$ and $\Phi_m = 35°$, which reflect the C3′-endo conformation typical for A-DNA and the C2′-endo conformation typical for B-DNA (Saenger, 1984). The pucker parameters are those commonly employed for the N and S conformers. Rapid interconversion, on the NMR time scale, is assumed between N and S conformers. Effective coupling constants $^3J_{HH}$ were calculated by

$$^3J_{HH} = (1 - f_S)^3J^N_{HH} + f_S{}^3J^S_{HH} \quad (1)$$

wherein f_S represents the mole fraction of the S conformer and $^3J^N_{HH}$ and $^3J^S_{HH}$ represent the coupling constants of the pure N and S conformers, respectively (Rinkel & Altona, 1987).

Figure 6 presents spectral simulations for a number of mixtures using a line width of 9 Hz. Clearly the absence of a H3′H2″ cross-peak, reflecting an active coupling constant ≤2.0 Hz (vide supra),[2] is indicative of a heavily S-biased equilibrium.

[2] We noticed that the line width and active coupling constants most strongly influence cross-peak intensities but the influence of passive coupling constants is not negligible, especially in those cases in which strong cancelation within the fine structure occurs.

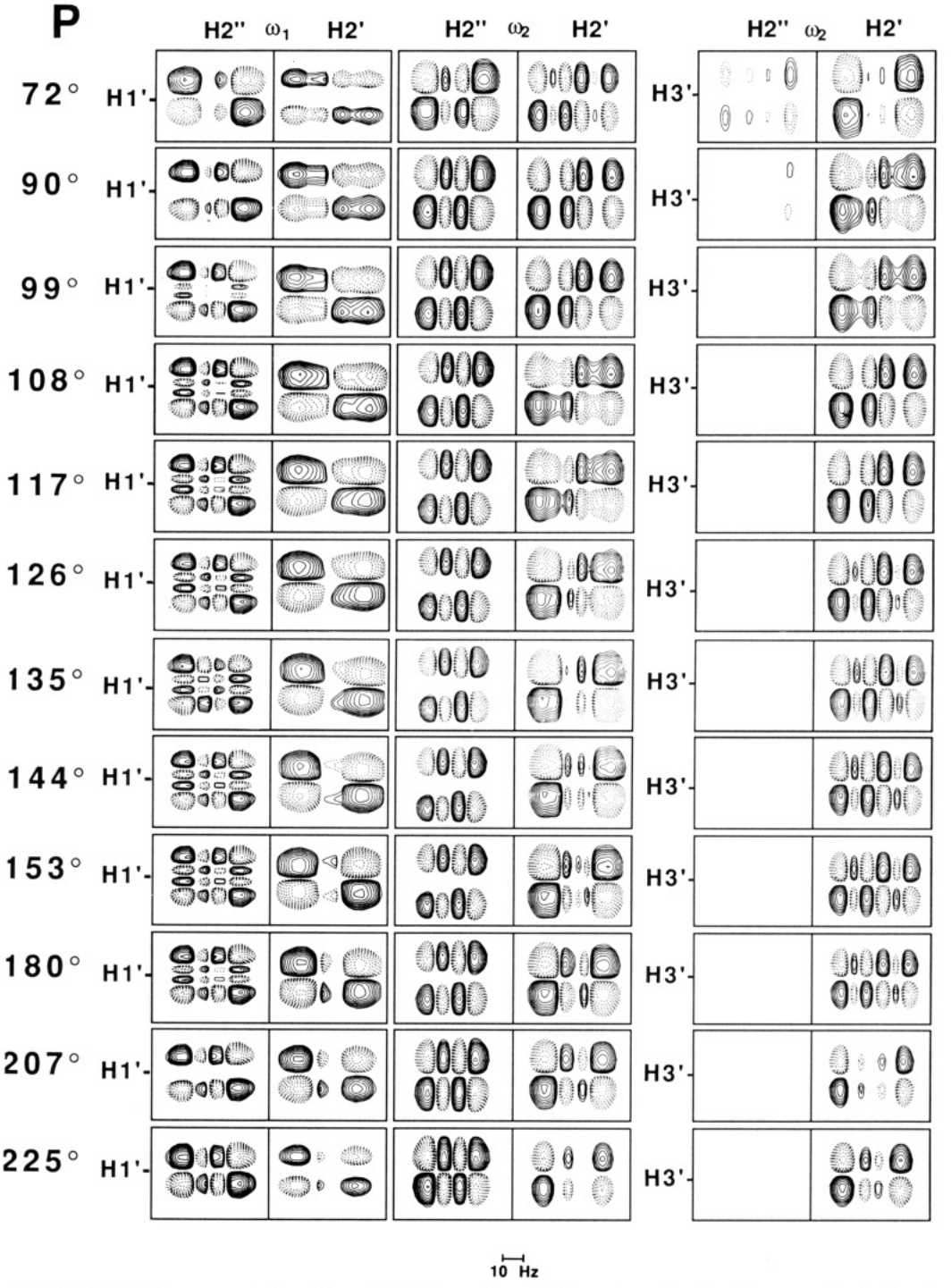

FIGURE 5: Simulated 2QF-COSY cross-peaks for different rigid deoxyribose conformations, described by a pseudorotation phase angle P and an amplitude $\Phi_m = 35°$: H1′H2″-ω_1, H1′H2′-ω_1, H1′H2″-ω_2, H1′H2′-ω_2, H3′H2″-ω_2, and H3′H2′-ω_2 from left to right. Resonance frequencies for the calculations were those of A3 in [d(GTATATAC)]$_2$. Chemical shift positions are indicated by the proton labels H1′, H2′, H2″, and H3′. $^2J_{2'2''}$ and $^3J_{3'P3'}$ are −14.0 and 5.8 Hz, respectively. All other vicinal coupling constants are shown in Table IV (Rinkel & Altona, 1987). Processing of the simulated data was achieved by using experimental 2QF-COSY parameters. A line width of 9 Hz was employed. Negative peaks are indicated by dashed lines. An empty box indicates that the corresponding cross-peak is of negligible intensity.

Table III: Vicinal Coupling Constants for Model Described in Figure 5

P (deg)	$J_{1'2''}$ (Hz)	$J_{1'2'}$ (Hz)	$J_{3'2''}$ (Hz)	$J_{3'2'}$ (Hz)	$J_{3'4'}$ (Hz)	P (deg)	$J_{1'2''}$ (Hz)	$J_{1'2'}$ (Hz)	$J_{3'2''}$ (Hz)	$J_{3'2'}$ (Hz)	$J_{3'4'}$ (Hz)
72	8.4	6.8	5.5	9.6	7.7	135	5.7	10.2	1.2	7.2	2.9
90	7.5	8.4	3.6	9.6	6.7	144	5.6	10.2	1.2	6.6	2.1
99	7.0	9.0	2.8	9.4	6.1	153	5.6	10.2	1.2	6.1	1.7
108	6.5	9.5	2.1	8.9	5.3	180	5.8	9.4	1.3	5.5	1.0
117	6.1	9.8	1.6	8.4	4.6	207	6.4	7.6	1.2	5.7	0.9
126	5.9	10.0	1.3	7.8	3.7	225	6.8	5.9	1.2	6.2	0.9

Juxtaposition of the series, computed with different line widths for both the rigid and the dynamic sugar puckers, revealed that a change in line width primarily affects the intensities of the fine structure components. However, in some

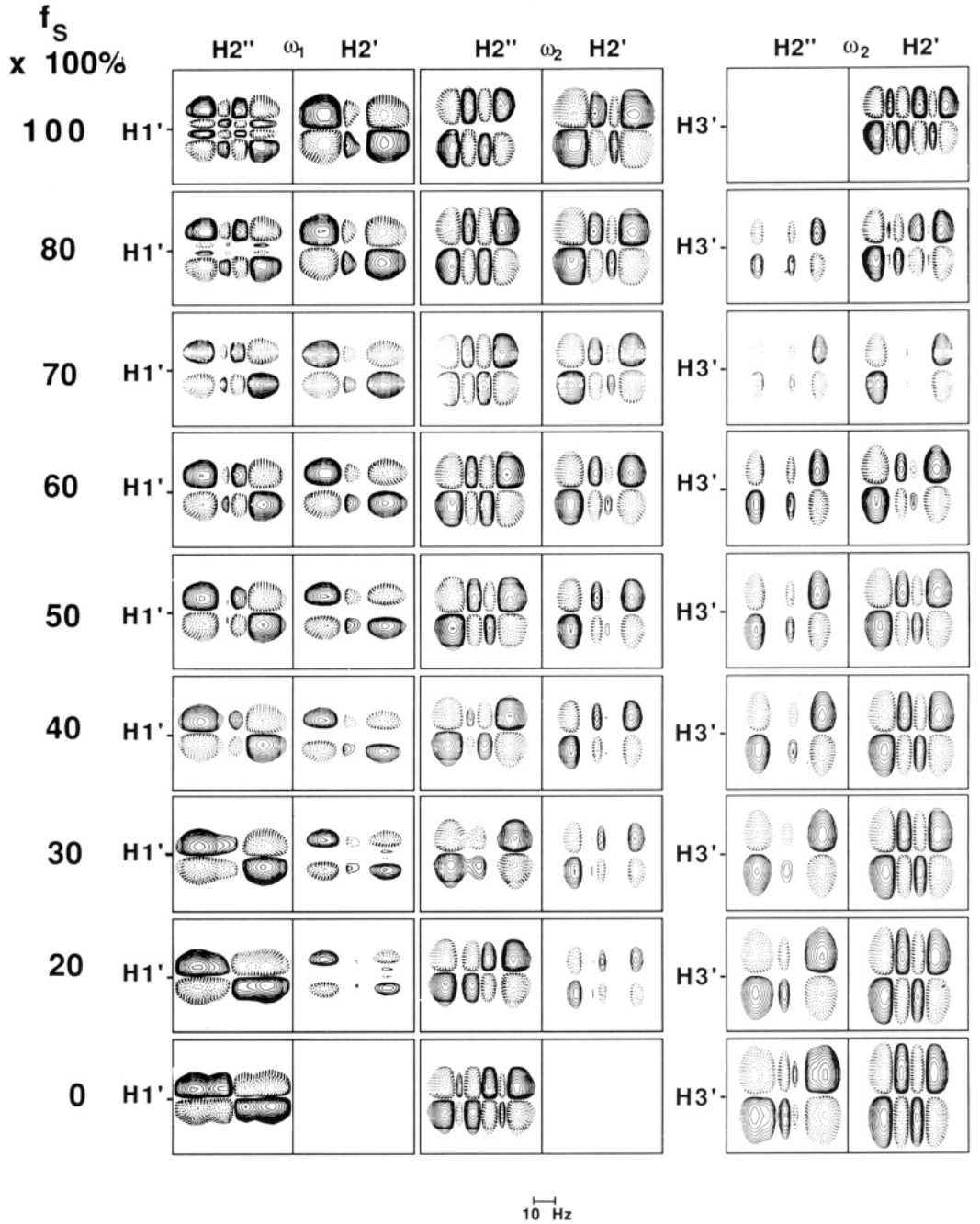

FIGURE 6: Simulated 2QF-COSY cross-peaks for different mixtures using a dynamic two-state model for deoxyribose, with $P_S = 162°$ and $P_N = 9°$ for the interconverting conformers ($\Phi_m = 35°$): H1′H2″-ω_1, H1′H2′-ω_1, H1′H2″-ω_2, H1′H2′-ω_2, H3′H2″-ω_2, and H3′H2′-ω_2 from left to right. Coupling constants were computed for different mole fractions f_S according to eq 1 (see text) (see Table V). Vicinal coupling constants for the conformers were taken from Rinkel and Altona (1987). For all other parameters, see Figure 5.

Table IV: Vicinal Coupling Constants for Model Described in Figure 6

f_S (×100)	$J_{1'2''}$ (Hz)	$J_{1'2'}$ (Hz)	$J_{3'2''}$ (Hz)	$J_{3'2'}$ (Hz)	$J_{3'4'}$ (Hz)	f_S (×100)	$J_{1'2''}$ (Hz)	$J_{1'2'}$ (Hz)	$J_{3'2''}$ (Hz)	$J_{3'2'}$ (Hz)	$J_{3'4'}$ (Hz)
100	5.8	9.5	1.3	5.5	1.0	40	6.9	4.7	6.3	6.5	5.1
80	6.2	7.9	3.0	5.8	2.4	30	7.1	3.9	7.2	6.7	5.8
70	6.4	7.1	3.8	6.0	3.0	20	7.3	3.1	8.2	6.9	6.4
60	6.6	6.3	4.7	6.2	3.7	0	7.7	1.5	9.7	7.2	7.8
50	6.8	5.5	5.5	6.4	4.4						

cases, especially if larger line widths are encountered, small components disappear or switch sign, highlighting the importance of proper line-width adjustment in the simulations. Figure 7 offers just a couple of examples in which a reasonable change in line width and coupling constants, reflective of a different conformation or a different conformer population ratio, could yield very similar 2QF-COSY spectral patterns. In our experiment, this ambiguity in the evaluation of peak shapes occurs more frequently when dealing with larger line widths; it was consequently impossible to use the simulation approach which was described recently (Celda et al., 1989). In this approach, the two prevailing coupling constants, $^3J_{1'2''}$ and $^3J_{3'2''}$, were varied within reasonable limits, keeping the other parameters involved constant. Celda et al. (1989) were able to match the most differentiated, indicative cross-peak (H1′H2′-ω_2) successfully. In the present case of [d(GTA-

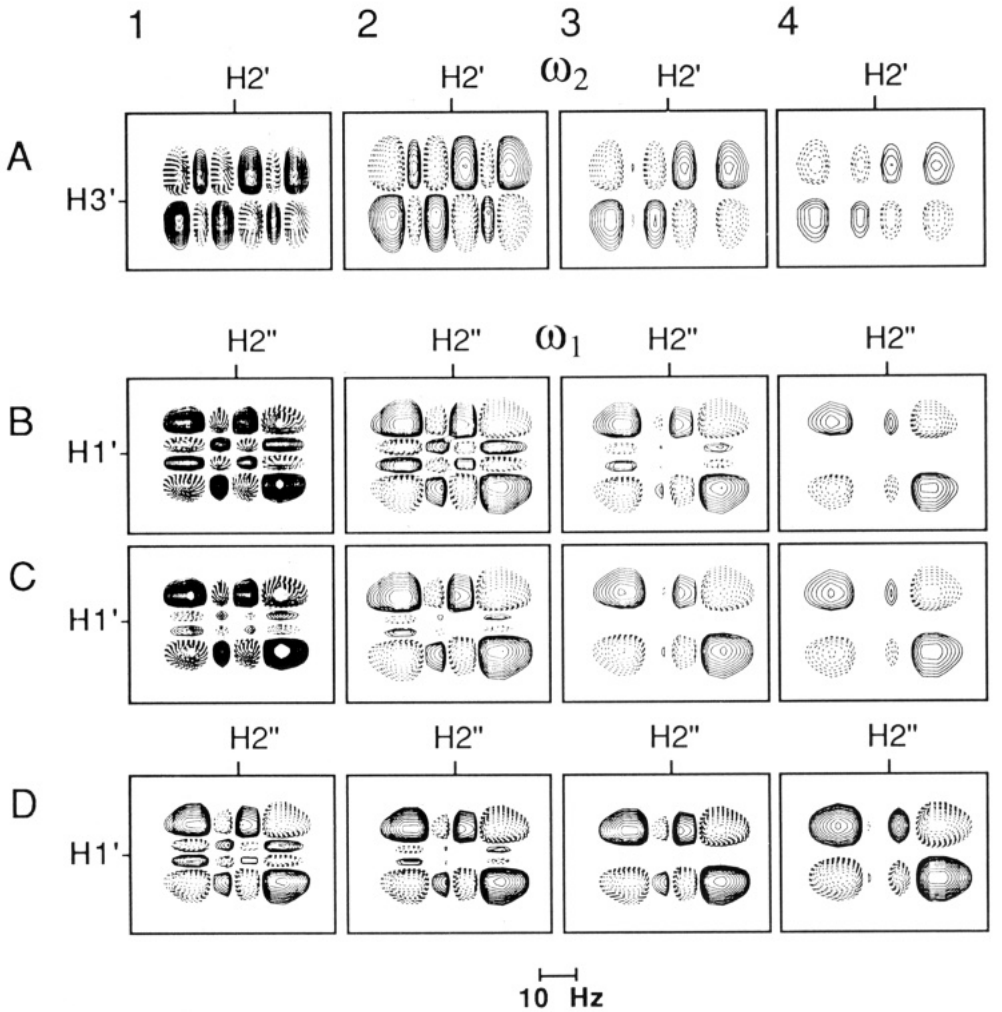

FIGURE 7: Interrelated influence of line width and coupling constants for the appearance of some simulated 2QF-COSY cross-peaks. (A) Simulated H3′H2′-ω_2 cross-peaks of a conformer utilizing coupling constants for $f_S = 1$ (see Figure 6) and line widths of (1) 7, (2) 9, (3) 11, and (4) 13 Hz. (B) Simulated H1′H2″-ω_1 cross-peaks for the same conformer and the same span of line widths as in (A). (C) Simulated H1′H2″-ω_1 cross-peaks for a mixture of conformers using coupling constants for $f_S = 0.8$ (see Figure 6) for the same span of line widths as in (A) and (B). (D) Simulated H1′H2″-ω_1 cross-peaks for different mixtures according to a three-state model, with a line width of 9 Hz (Table VI).

Table V: Compositions of N and S Conformers and Vicinal Coupling Constants for Model Described in Figure 7[a]

	% N (P = 9°)	% S (P = 126°)	% S (P = 162°)	$^3J_{1'2''}$ (Hz)	$^3J_{1'2'}$ (Hz)	$^3J_{3'2''}$ (Hz)
1	10	72	18	6.1	9.2	2.1
2	20	64	16	6.3	8.2	3.0
3	30	56	14	6.6	7.6	3.6
4	40	48	12	6.8	6.7	4.7

[a] $^2J_{2'2''} = -14.0$ Hz for all simulations.

TATAC)]$_2$, the H1′H2′ cross-peaks were not very distinguishable, exhibiting only four broad components. Thus, we were forced to assess the quality of a match for a special set of all involved coupling constants by comparing all six available simulated peaks with the experimental ones. Since complete sets of coupling constants would need to be tested, computing random combinations seemed rather hopeless. Instead, different sets of coupling constants were used, reflecting sugar puckers which were reasonable extensions of the closest result obtained from the introductory series of simulations, both for rigid and for dynamic (two-state) puckers (Figures 5 and 6). For these simulations, different values for $^2J_{2'2''}$ had to be covered (−13.0, −14.0, and −15.0 Hz), although this parameter is not related to the deoxyribose conformation. $^2J_{2'2''}$ is expected to be close to −14.0 Hz (Davis, 1978); however, in some cases, especially for matching some cross-peaks along the ω_1 dimension, it was crucial to adjust the geminal coupling constant to −15.0 Hz. $^3J_{^{31}P3'}$ also affects the H3′H2′ and H3′H2″ cross-peaks along the ω_1 dimension, but as it does not directly pertain to the deoxyribose conformation, a fixed value was used (5.8 Hz).

In the course of trying to fit simulated spectra to experimental spectra, it became obvious that within the oligonucleotide there are variations in line width. This should not be too surprising as the line width for any particular resonance will be dependent on the proton environment and molecular motions of the proton of interest. The smallest line widths were found for terminal residues G1 and C8 (6–9 Hz), while nonterminal residues exhibited the biggest variation (7–12 Hz). The H1′ line width was generally the smallest (6–7 Hz). In all casess, except G1, the H2′ line width was 2–3 Hz larger than that for H2″. While this may initially be surprising, it is actually quite reasonable since all H2′ protons experience a similar proton environment which is different from that for

Table VI: Deoxyribose Coupling Constants of [d(GTATATAC)]$_2$ Determined from Quantitative Simulation

residue	$^3J_{1'2''}$ (Hz)	$^3J_{1'2'}$ (Hz)	$^3J_{3'2''}$ (Hz)	$^3J_{3'2'}$ (Hz)	$^3J_{3'4'}$ (Hz)	$^3J_{2'2''}$ (Hz)
G1	6.6 ± 0.1	6.3 ± 0.5	4.7 ± 0.4	6.3 ± 0.2	3.7 ± 0.5	−14.5 ± 0.5
T2	6.1 ± 0.1	8.7 ± 0.5	2.5 ± 0.4	6.7 ± 0.1	3.0 ± 0.2	−14.5 ± 0.5
A3	6.3 ± 0.2	7.9 ± 0.5	3.0 ± 0.5	6.9 ± 0.2	3.3 ± 0.3	−14.5 ± 0.5
T4	6.3 ± 0.2	7.9 ± 0.5	3.0 ± 0.5	6.9 ± 0.2	3.3 ± 0.3	−14.5 ± 0.5
A5	6.3 ± 0.2	7.9 ± 0.5	3.0 ± 0.5	6.9 ± 0.2	3.3 ± 0.3	−14.5 ± 0.5
T6	6.3 ± 0.2	7.9 ± 0.5	3.0 ± 0.5	6.9 ± 0.2	3.3 ± 0.3	−14.5 ± 0.5
A7	6.3 ± 0.2	7.9 ± 0.5	3.0 ± 0.5	6.9 ± 0.2	3.3 ± 0.3	−14.5 ± 0.5
C8	(6.6 ± 0.1)[a]	(6.3 ± 0.5)	(4.7 ± 0.4)	(6.3 ± 0.2)	(3.7 ± 0.5)	(−14.5 ± 0.5)

[a] Parentheses indicate tentative assignment.

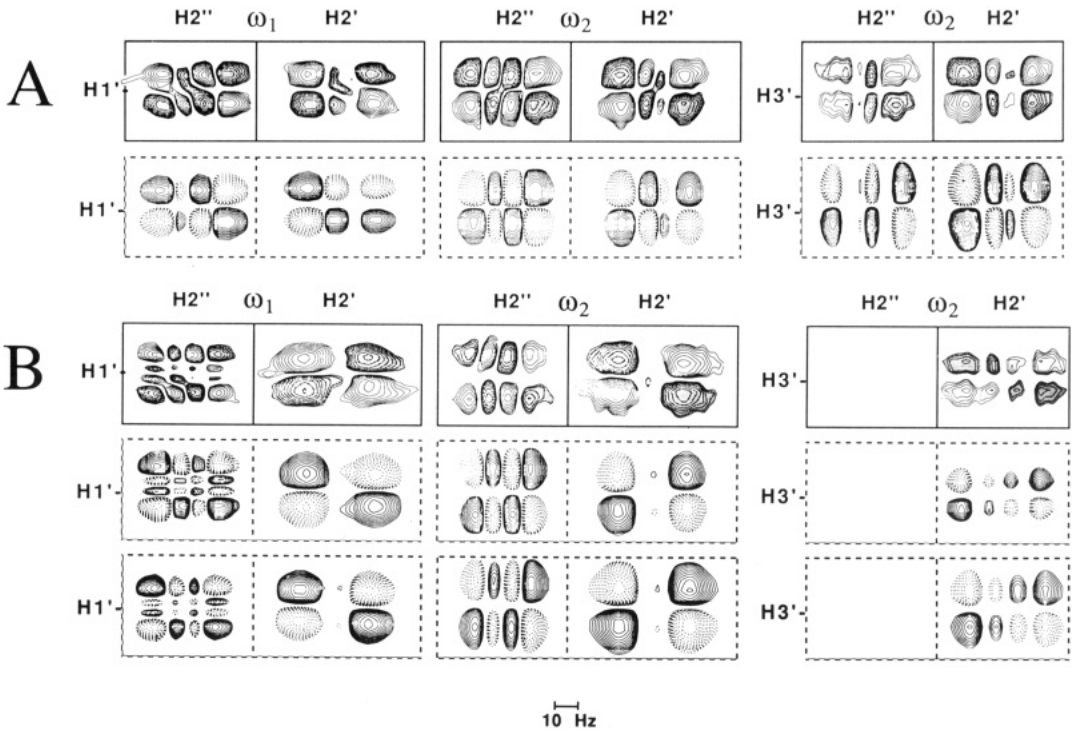

FIGURE 8: Comparison of experimental 2QF-COSY cross-peaks (solid boxes) and best-fit simulations (dashed boxes). (A) Juxtaposition of the experimental and simulated 2QF-COSY cross-peaks for G1. Coupling constants used for the simulation correspond to those of a two-state model with P_S = 162°, P_N = 9°, and f_S = 0.6 (see Figure 6). (B) Juxtaposition of the experimental and two sets of simulated 2QF-COSY cross-peaks for T2 calculated by using a two-state model (P_S = 144°, P_N = 9°, f_S = 0.85) (upper simulation) and a three-state model (P_S = 162°, 52%; $P_{S'}$ = 126°, 33%; P_N = 9, 15%) (lower simulation). H1′H2″-ω_1, H1′H2′-ω_1, H1′H2″-ω_2, H1′H2′-ω_2, H3′H2″-ω_2, and H3′H2′-ω_2 are shown from left to right. Actual chemical shifts and individual line widths were used. Chemical shift positions are indicated by the proton labels H1′, H2′, H2″, and H3′.

the H2″ protons, assuming a B-DNA family structure. However, the environment for H2′ and H2″ of the terminal nucleotides differs from that of nonterminal nucleotides, explaining the exceptional behavior of G1 H2′ and G1 H2″. Intrinsic H3′ line widths were assumed to be the same as for H1′; it was not possible to directly determine this parameter due to interference from $^3J_{^{31}P3'}$.

A comparison of the experimental cross-peaks in Figure 4 with simulations for the static model in Figure 5 reveals that a rigid single sugar pucker does not apply for any of the nucleotides. However, from Figure 6 it is obvious that the G1 experimental peaks find their match with simulations using the 60% S mixture. The simulation for this mixture was repeated for the actual G1 chemical shifts but did not lead to a different conclusion concerning the sugar pucker. Other mixtures close to 60% S were tried to determine the uncertainty of the more or less subjective visual matching of peaks. It turned out that simulated peaks for mixtures containing between 55% and 65% S conformer are virtually indistinguishable from the original 60% S mixture. The resulting coupling constants are presented in Table VI with the estimated error, which can be different for each of the coupling constants.

No satisfactory match could be gleaned from Figure 6 for the other nucleotides. Two different ways to proceed were tried. To match the T2 cross-peaks, simulated spectra for different series of mixtures were computed by using a variety of pseudorotation phase angles for the major conformer. The best fit was obtained for a 85% S mixture with P_S = 144° and Φ_m = 35° (Figure 8). However, employing two different conformers in the S range of pseudorotation, with P_S = 162°, P_S = 126°, and both with Φ_m = 35°, also resulted in a mixture which provided good simulated peaks: 52% S (P_S = 162°), 33% S′ ($P_{S'}$ = 126°), and 15% N (P_N = 9°). The two-state and three-state models provide essentially the same sets of coupling constants and, consequently, the same simulated spectra. Therefore, we cannot, on this basis, distinguish between a two-state model employing a less conventional P_S value or a three-state model employing two S conformers, the dominant one of which has a conventional P_S. Of course, the three-state model has more parameters and thus should be fit more readily. In fact, it is likely that other variations of the parameters would yield satisfactory fits if pseudorotation angles, amplitudes, and conformers populations were all treated as variables. A prudent course would be to invoke Occam's Razor and designate the two-state model, but low conforma-

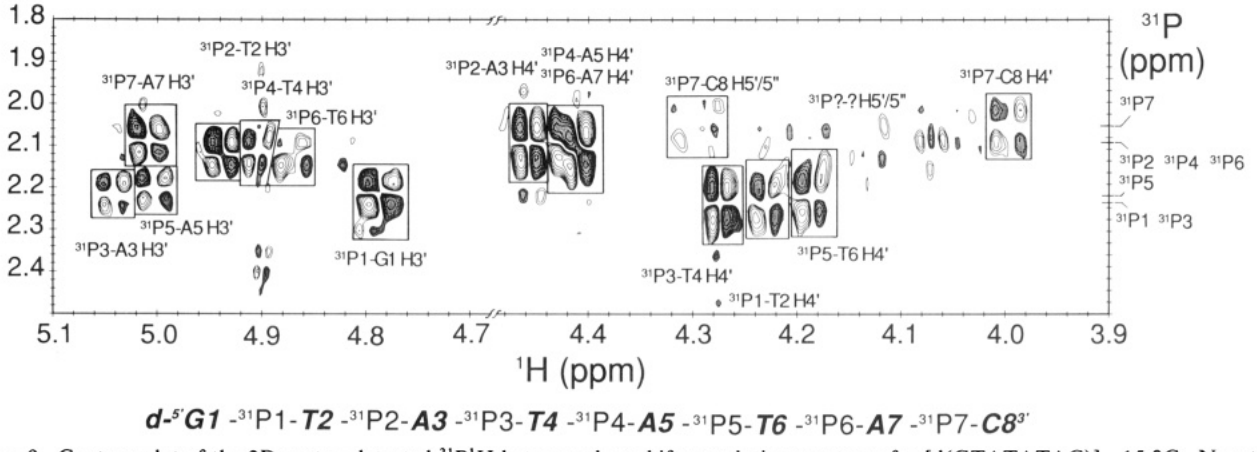

FIGURE 9: Contour plot of the 2D proton-detected $^{31}P^{1}H$ heteronuclear shift correlation spectrum for $[d(GTATATAC)]_2$, 15 °C. Negative peaks are indicated by the shaded regions. Assignments for the phosphorus resonances, labeled in the figure, are as follows: $^{31}P7$, 2.09 ppm; $^{31}P2$, $^{31}P4$, $^{31}P6$, 2.10_5 ppm; $^{31}P5$, 2.21_5 ppm; $^{31}P1$, 2.21_5 ppm. ^{31}P chemical shifts are given relative to TMP.

tional barriers could mean that a three-state model is more realistic. Indeed, molecular dynamics simulations carried out with the sequence $[d(CGCGAATTCGCG)]_2$ revealed recently (Kollman & Rao, 1989) that sugar puckers in the middle range of the pseudorotation phase cycle (P = 54–126°) do occur and sometimes represent up to 30% of the observed sugar puckers. These results support the idea of involving a third conformer to describe dynamic sugar pucker and show that the energy barriers between conformers exhibiting puckers located in S and N pseudorotation half-cycles are lower than commonly assumed.

The experimental cross-peaks of the core of the duplex, A3 to A7, strongly resemble those of T2. The only visible deviation accessible by simulation is the negligible intensity of the inner components in the H1′H2″-ω_1 cross-peaks of A3 to A7. Two different minor variations in the parameter sets used for T2 provided simulated peak shapes with the desired characteristics. On the one hand, an increase in line width along the ω_2 dimension of more than 2 Hz eliminates the innermost components of the fine structure and decreases significantly the intensity of the left inner peaks of the remaining components (cf. Figure 7). Alternatively, reducing the difference between the two prevalent coupling constants along ω_2, $^3J_{1'2''}$ and $^3J_{1'2'}$, by 0.5–1.5 Hz, corresponding to a 5–10% increase of the N conformer contribution in the aforementioned two- and three-state model, extinguishes the small inner peaks but hardly affects the intensity of the left inner component of the outer rows (cf. Figure 7). The actual experimental peak shapes suggest a composite effect consisting of a slight line-width increase and a 5% increase in the N conformer population. While these modifications improve the visual fitting of spectra, they are not firm, as there is a significant range for the individual coupling constants. It should be mentioned that these minor changes in the coupling constants could also be caused by deviations in the amplitude of pucker Φ_m from 35° as well as by changes in P and the conformer ratio. The error range of the present results, arising from fairly undifferentiated peaks due to large line width, made it impossible to include the amplitude of pucker as a parameter in the simulations; it was therefore set to a fixed value. However, it is not likely to deviate much according to numerous X-ray studies (Saenger, 1984).

A satisfactory simulation for the strongly overlapped cross-peaks of C8 was not achieved, but the presence of a H3′H2″ cross-peak and the sum of $^3J_{1'2'}$ and $^3J_{1'2''}$ identical with that of G1 suggest a pucker similar to G1. Increased conformational flexibility of the 3′-terminal nucleotide was also found in other studies (Orbons & Altona, 1986; Celda et al., 1989).

All results of the present study are consistent with the observed intensities for the H3′H4′ cross-peaks, which were not included in the simulation. All these peaks are observed with medium intensity. G1 and C8 gave H3′H4′ peaks with somewhat higher intensity according to their larger values for $^3J_{3'4'}$.

The coupling constants and associated errors listed in Table III reflect the assessment of the general appearance of the 2QF-COSY cross-peaks. However, there were some irregularities within the fine structures, which could not be simulated. For example, some peaks were skewed from the perpendicular axis or exhibited an unsymmetrical distribution of intensities. Among these irregularities, the distorted shape of the H3′H2′ peaks of T4 and T6 is notable, since, together with some intensity variations in H1′H2″ cross-peaks, this seems to be the only hint from the 2QF-COSY spectra for conformational differences between T and A sugars within the inner part of the duplex.

Structural Implications from the Proton-Detected $^{31}P^{1}H$ Heteronuclear Shift Correlation Experiment. Knowledge of the H3′ and H4′ chemical shifts enabled assignment of all ^{31}P resonances (Figure 9), although a different buffer was used for the sample with consequent minor deviations in proton chemical shifts. All $^{31}PH3'$ and $^{31}PH4'$ cross-peaks were observed, but not all $^{31}PH5'/5''$ cross-peaks, as typical for a large variety of B-DNA duplexes (Gorenstein, 1983; Wüthrich, 1986). Separations between the individual components of the four-component cross-peaks represent sums of coupling constants, thus enabling no more than a qualitative assessment of the parameters associated with the backbone conformation.

There are no large differences between the observable ^{31}P cross-peaks. The cross-peak of $^{31}P1$ with G1 H3′ exhibits a slightly larger intensity than the others presumably due to a smaller line width and a comparably larger sum of G1 H3′ coupling constants to protons. The other terminal phosphorus in the duplex, $^{31}P7$, shows the least intense cross-peak in the H4′ region, possibly indicating backbone deviations at the 3′-terminus. Only traces of cross-peaks to H5′/H5″protons emerge, presumably due to very small coupling constants and cancellation effects caused by the narrow chemical shift distribution of the H5′/5″ protons. It is quite interesting that resolved cross-peaks are found for the $^{31}P2$, $^{31}P4$, $^{31}P6$, and $^{31}P7$ resonances, which are at TA junctions and the A7C8 terminal junction, respectively. For the remaining ^{31}P resonances, H4′ and H5′/5″ regions are more overlapped, but if

the pertinent backbone torsion angles are essentially the same at all junctions as for simple B-DNA, at least some ^{31}PH5′/5″ cross-peak intensity should be detectable. The alternating torsion angles found in the analysis of [d(GGTATACC)]$_2$ (Zhou et al., 1987) would indeed yield a larger ^{31}PH5′/5″ coupling constant in the case of TA junctions, corroborating the present finding.

Another hint of a difference between AT and TA junctions arises from a ^{31}P chemical shift comparison. Essentially three different kinds of chemical shifts are observed, each with a very small range of ≈0.15 ppm. One arises from ^{31}P1, ^{31}P3, and ^{31}P5, located in AT junctions. ^{31}P2, ^{31}P4, and ^{31}P6 positions exhibit another unique chemical shift, and the ^{31}P7 resonance has the smallest value. No quantitative evaluation is possible at the present time, but there is substantial support correlating ^{31}P chemical shifts and phosphodiester backbone conformation (Gorenstein & Kar, 1975; Gorenstein et al., 1990). Therefore, ^{31}P chemical shifts and ^{31}PH5′/5″ cross-peak variations support the notion of backbone differences at AT and TA junctions.

Conclusions

Scalar coupling-based 2D NMR spectra, including 2QF-COSY cross-peaks, of [d(GTATATAC)]$_2$ were not amenable to attempts to extract coupling constants directly due chiefly to significant line widths. Quantitative spectral simulation of the 2QF-COSY spectra was the only method enabling the elucidation of sugar pucker. H1′H2′-ω_2, H1′H2″-ω_2, H1′H2′-ω_1, H1′H2″-ω_1, H3′H2′-ω_2, and H3′H2″-ω_2 cross-peaks were simulated and visually compared with experimental ones. Simulations were performed utilizing coupling constant sets with different pseudorotation angles P for both rigid and dynamic sugar puckers. In the case of dynamic models, the conformer composition was varied systematically to find the best matched simulations between the experimental and simulated cross-peaks. A proper line-width adjustment for the simulation turned out to be crucial. Terminal residues were found to exhibit smaller line widths than nonterminal ones. Even within a particular deoxyribose, different line widths existed; e.g., H2″ generally exhibited a smaller line width than H2′. As with direct extraction methods, line width turned out to be the major limitation of the simulation method, since valuable fine structure is obscured by increasing line widths. In the present case, the cross-peak which generally should be the most informative, i.e., H1′H2′-ω_2, happened to have the largest line width. Rigid sugar conformations could be excluded for all nucleotides. The classical two-state model provided an unambiguous sugar pucker description for the terminal residues, G1 and tentatively C8: a conformational mixture containing 60% C2′-endo and 40% C3′-endo conformers. For T2, the contribution of the S conformer increased to about 85%. However, the pseudorotation phase angle had to be changed to P_S = 144°, or a third minor conformer with P_S = 126° had to be involved. For the core of the duplex, A3 to A7, the situation was similar to that of T2, but the N conformer contribution is increased slightly (5%). An error range of ±5% in conformer population, due mainly to broad lines, is presumably the reason for not observing any differentiation within the TATATA part of the oligonucleotide. However, peak shape peculiarities of the H3H2′-ω_2 cross-peaks of T4 and T6, not expressable by simulation, suggested a possible small alternation in sugar pucker from T and A sugars. ^{31}P^{1}H heteronuclear shift correlation spectra exhibited alternating chemical shifts and coupling constants, again suggestive of a variation in phosphodiester backbone conformation from TA to AT. However, the undramatic results would generally imply that the variation is not too large.

Acknowledgments

We thank Mark Day and Dr. Pamela Mills for improvements in the NMR data processing software and Dr. Hans Widmer for making the SPHINX and LINSHA programs available.

References

Altona, C. (1982) *Recl.: J. R. Neth. Chem. Soc. 101*, 413–433.

Altona, C., & Sundaralingam, M. (1972) *J. Am. Chem. Soc. 94*, 8205–8212.

Arnott, S., Chandrasekaran, R., Puigjaner, L. C., Walker, J. K., Hall, I. H., Birdsall, D. L., & Ratcliff, R. L. (1983) *Nucleic Acids Res. 11*, 1457–1474.

Bax, A., & Lerner, L. (1988) *J. Magn. Reson. 79*, 429–438.

Boelens, R., Scheek, R. M., Dijkstra, K., & Kaptein, R. (1985) *J. Magn. Reson. 62*, 371–386.

Broido, M. S., Zon, G., & James, T. L. (1984) *Biochem. Biophys. Res. Commun. 119*, 663–670.

Celda, B., Widmer, H., Leupin, Chazin, W. L., Denny, . A., & Wüthrich, K. (1989) *Biochemistry 28*, 1462–1471.

Chary, K. V. R., Hosur, R. V., Govil, G., Chen, C., & Miles, H. T. (1988) *Biochemistry 27*, 3858–3867.

Chary, K. V. R., Modi, S., Hosur, R. V., Govil, G., Chen, C., & Miles, H. T. (1989) *Biochemistry 28*, 5240–5249.

Davies, D. B. (1978) *Prog. Nucl. Magn. Reson. Spectrosc. 12*, 135–225.

de Leeuw, F. A. A. M., & Altona, C. (1982) *J. Chem. Soc., Perkin Trans. 2*, 375–384.

de Leeuw, F. A. A. M., Haasnoot, C. A. G., & Altona, C. (1980) *Isr. J. Chem. 20*, 108–126.

de Leeuw, F. A. A. M., van Beuzekom, A. A., & Altona, C. (1983) *J. Comput. Chem. 4*, 438–448.

Feigon, J., Wright, J. M., Leupin, W., Denny, W. A., & Kearns, D. R. (1982) *J. Am. Chem. Soc. 104*, 5540–5541.

Fegon, J., Leupin, W., Denny, W. A., & Kearns, D. R. (1983) *Biochemistry 22*, 5943–5951.

Freeman, R., Kempsell, S. P., & Levitt, M. H. (1980) *J. Magn. Reson. 38*, 453–479.

Gorenstein, D. G. (1983) *Phosphorous-31 NMR Principles and Applications*, Academic Press, Orlando, FL.

Gorenstein, D. G., & Kar, D. (1975) *Biochem. Biophys. Res. Commun. 65*, 1073–1080.

Gorenstein, D. G., Schroeder, D. A., Fu, L. M., Metz, J. T., Roongta, M. A., & Jones, C. R. (1990) *Biochemistry* (in press).

Griesinger, C., Sørensen, O. W., & Ernst, R. R. (1985) *J. Am. Chem. Soc. 107*, 6394–6396.

Hosur, R. V., Govil, G., & Miles, H. T. (1988) *Magn. Reson. Chem. 26*, 927–944.

Jamin, N., James, T. L., & Zon, G. (1985) *Eur. J. Biochem. 152*, 157–166.

Kessler, H., Müller, A., & Oschkinat, H. (1985) *Magn. Reson. Chem. 23*, 844–852.

Kollman, P. A., & Rao, S. N. (1989) *Biopolymers* (in press).

Marion, D., & Woüthrich, K. (1983) *Biochem. Biophys. Res. Commun. 113*, 967–974.

Maudsley, A. A., & Ernst, R. R. (1977) *Chem. Phys. Lett. 50*, 366–372.

Neuhaus, D., Wagner, G., Vâsâk, M., Kägi, J. H. R., & Wüthrich, K. (1985) *Eur. J. Biochem. 151*, 257–273.

Orbons, L. P. M., & Altona, C. (1986) *Eur. J. Biochem. 160*, 141–148.

Piantini, V., Sørensen, O. W., & Ernst, R. R. (1982) *J. Am. Chem. Soc. 104*, 6800-6801.
Rinkel, L. J., & Altona, C. (1987) *J. Biomol. Struct. Dyn. 4*, 621-649.
Saenger, W. (1984) *Principles of Nucleic Acid Structure*, Springer, New York.
Scheek, R. M., Russo, N., Boelens, R., Kaptein, R., & van Boom, J. H. (1983) *J. Am. Chem. Soc. 105*, 2914-2916.
Scheek, R. M., Boelens, R., Russo, N., van Boom, J. H., & Kaptein, R. (1984) *Biochemistry 23*, 1371-1376.
Shakked, Z., Rabinovich, D., Cruse, W. B. T., Egert, E., Kennard, O., Sala, G., Salisbury, S. A., & Viswamitra, M. A. (1981) *Proc. R. Soc. London, Ser. B B213*, 479-482.
Shakked, Z., Rabinovich, D., Kennard, O., Cruse, W. B. T., Salisbury, S. A., & Viswamitra, M. A. (1983) *J. Mol. Biol. 166*, 183-201.
States, D. J., Haberkorn, R. A., & Ruben, D. J. (1982) *J. Magn. Reson. 48*, 286-292.
Suzuki, E., Pattabiraman, N., Zon, G., & James, T. L. (1986) *Biochemistry 25*, 6854-6865.
Widmer, H., & Wüthrich, K. (1986) *J. Magn. Reson. 70*, 270-279.
Widmer, H., & Wüthrich, K. (1987) *J. Magn. Reson. 74*, 316-336.
Wiliamson, D., & Bax, A. (1988) *J. Magn. Reson. 76*, 174-177.
Wüthrich, K. (1984) *NMR of Proteins and Nucleic Acids*, Wiley, New York.
Zhou, N., Bianucci, A. M., Pattabiraman, N., & James, T. L. (1987) *Biochemistry 26*, 7905-7913.
Zhou, N., Manogaran, S., Zon, G., & James, T. L. (1988) *Biochemistry 27*, 6013-6020.

Differential Effect of Insulin and Epidermal Growth Factor on the mRNA Translocation System and Transport of Specific Poly(A+) mRNA and Poly(A-) mRNA in Isolated Nuclei†

Heinz C. Schröder,*,‡ Rosemarie Wenger,‡ Durdica Ugarković,‡ Klaus Friese,§ Michael Bachmann,‡ and Werner E. G. Müller‡

Institut für Physiologische Chemie, Universität, Duesbergweg 6, D-6500 Mainz, Federal Republic of Germany, and Klinikum Mannheim, Theodor Kutzer Ufer, D-6800 Mannheim, Federal Republic of Germany

Received May 31, 1989; Revised Manuscript Received October 6, 1989

ABSTRACT: The efficiency of efflux of rapidly labeled poly(A)-containing mRNA from isolated rat liver nuclei was found to be modulated by insulin and epidermal growth factor (EGF) in a biphasic but opposite way. At physiological concentrations (10 pM insulin and 1 pM EGF), maximal stimulation of the transport rate by insulin (to 137%) and maximal inhibition by EGF (to 69%) were obtained; at higher concentrations (>100 pM and >10 pM, respectively), the amount of poly(A)-containing mRNA released into the postnuclear supernatant was nearly identical with the level found in untreated nuclei (=100%). Using mRNA entrapped into closed nuclear envelope (NE) vesicles as a model system, it was found that the modulation of nuclear efflux of mRNA by the two growth factors occurs at the level of translocation through the nuclear pore. The NE nucleoside-triphosphatase (NTPase) activity, which is thought to mediate nucleocytoplasmic transport of at least some mRNAs, responded to insulin and EGF in the same manner as the mRNA transport rate. The increase in NTPase activity caused by insulin and the decrease in NTPase activity caused by EGF were found to be due to changes of the maximal catalytic rate; the Michaelis constant of the enzyme remained almost constant. Investigating the effect of the two growth factors on transport of specific mRNAs, poly(A)-containing actin mRNA was found to display the same alteration in efflux rate as rapidly labeled, total poly(A)-containing mRNA. In contrast, efflux of histone H4 mRNA, which lacks a 3'-poly(A) sequence, decreased in response to insulin and reached minimum levels at the same concentration at which maximum levels of actin mRNA transport rate were obtained. Studying the mechanism of action of insulin and EGF on NE mRNA translocation system, insulin was found to cause an enhancement of NE-associated phosphoprotein phosphatase activity, resulting in a dephosphorylation of the NE poly(A) binding site (=mRNA carrier) and, hence, in a decrease in its affinity to poly(A) [the poly(A) binding affinity of the poly(A)-recognizing mRNA carrier within the envelope is increased after phosphorylation]. EGF, on the other hand, stimulated the protein kinase, which phosphorylates the carrier, and, hence increased the NE poly(A) binding affinity. Because the stage of phosphorylation of the mRNA carrier (which is coupled with the NTPase within the intact NE structure) is inversely correlated with the activity of the NTPase, an enhancement of poly(A)-containing mRNA transport rate by insulin and an inhibition by EGF are observed.

Transport of mRNA from the nucleus to the cytoplasm across the nuclear envelope (NE)[1] can be subdivided into three steps (Schröder et al., 1987a; Agutter, 1988): (1) release of mRNA from the intranuclear binding site (nuclear matrix; Schröder et al., 1987b); (2) translocation of the mRNA

† This work was supported by Grants Schr 277/2-1 and Mu 348/7-7 from the Deutsche Forschungsgemeinschaft.
‡ Institut für Physiologische Chemie.
§ Klinikum Mannheim.

[1] Abbreviations: EGF, epidermal growth factor; NE, nuclear envelope; NTPase, nucleoside-triphosphatase; PK, protein kinase; poly(A+) mRNA, poly(A)-containing mRNA; poly(A-) mRNA, poly(A)-free mRNA; PPH, phosphoprotein phosphatase; $PhMeSO_2F$, phenylmethanesulfonyl fluoride; EGTA, [ethylenebis(oxyethylenenitrilo)]-tetraacetic acid; $NaDodSO_4$, sodium dodecyl sulfate.

0006-2960/90/0429-2368$02.50/0